Research Article | Vol. 11, No. 11 / 1 Nov 2021 / Optical Materials Express 3833
Optical Materials EXPRESS

High-sensitivity multi-channel refractive-index sensor based on a graphene-based hybrid Tamm plasmonic structure

JINLEI HU,[1] YULAN HUANG,[1] YUXUAN CHEN,[1] ZHENG-DA HU,[1] JINGJING WU,[1] AND JICHENG WANG[1,2,*]

[1]School of Science, Jiangsu Provincial Research Center of Light Industrial Optoelectronic Engineering and Technology, Jiangnan University, Wuxi 214122, China
[2]State Key Laboratory of Applied Optics, Changchun Institute of Optics, Fine Mechanics and Physics, Chinese Academy of Sciences, Changchun 130033, China
*jcwang@jiangnan.edu.cn

Abstract: In this paper, we propose a high-performance refractive-index sensor at a near-infrared band based on a hybrid Tamm structure. The optical properties of this graphene-based hybrid Tamm plasmonic structure are analyzed and investigated by using the transfer matrix method (TMM). Due to the excitation of the guide mode resonance (GMR) and Tamm plasmon polariton (TPP) resonance, the structure can realize multi-channel perfect absorption. This structure can be utilized as a refractive index sensor because the position of the absorption peak is sensitive to the refractive index of the ambient layer. Therefore, we obtain the sensitivity to 950 nm per refractive index unit (nm/RIU) and figure of merit (FoM) of 161 RIU^{-1} after studying the performance under different structural parameters. We believe that the proposed configuration is expected to be used to manufacture high-performance biosensors or gas sensor devices and other related applications in the near-infrared band.

© 2021 Optical Society of America under the terms of the OSA Open Access Publishing Agreement

1. Introduction

Tamm plasmon polariton (TPP) is a unique surface mode that is supported at the interface of a metal film and distributed Bragg reflector (DBR), which exhibits a decaying field envelope in metal as well as in th DBR [1]. It has intriguing characteristics like light control and operation, so it is widely used in the design of new generation photonic devices [1–5]. TPP was predicted as early as 1932 [2], and the existence of Tamm state in superlattice was first confirmed in 1990 [3]. Subsequently, Kavokin et al. firstly proposed optical TPPs in 2005 [4]. Unlike surface plasmon polariton (SPP), with the dispersion within the light cone, TPP can be directly excited by both TM- and TE- polarized light from free space, without the need for a specific incident angle or dispersion regulator [1,4]. And the spectral width of TPPs is very narrow, which is one order of magnitude smaller than that of SPPs. Therefore, TPP has a larger resonance mode when the local field is enhanced. In addition, TPP has very low transmission loss and high-quality factor, which is very suitable for optical modulation and sensitive detection [5,11–14]. The application of TPPs for refractive index sensors has been demonstrated [6–9]. Applications of TPP-based refractive index sensors for fluid detection and temperature sensing are presented in Refs. [10,11], respectively. Also, TPP resonance modes have been used in combination with propagating surface plasmonic modes to improve the performance of refractive index sensors using near-infrared multimode optical fibers [12,13]. And some researchers have studied the application of magneto-optical optical Tamm state in detection [13–11].

Graphene, an attractive, atomically thin carbon material that can replace metals, has shown a plasmonic reaction in the infrared region, featuring a greatly enhanced electric field and ultra-fast optical tunability [15–19]. Surface plasmons (SPs) in graphene are electromagnetic waves that

#440987 https://doi.org/10.1364/OME.440987
Journal © 2021 Received 18 Aug 2021; revised 7 Oct 2021; accepted 12 Oct 2021; published 20 Oct 2021

Optical Materials EXPRESS

propagate along the surface of the graphene due to the infrared light-induced oscillation of surface charges, which can effectively enhance optical absorption [20–23]. To better improve the light absorption performance of the graphene monolayer, a simple method of guided mode resonance (GMR) can be introduced to maintain SPs [15–24].

In this paper, we first studied a dual-Tamm structure to achieve a multi-channel absorption effect by using TPP resonance. Then, due to the excellent optical and electrical properties of graphene, we combine graphene-based grating with the dual-Tamm structure and introducing GMR resonance to achieve absorption effects of different modes. Moreover, the TPP resonance frequency is sensitive to the change in the ambient refractive index of the Tamm structure. The sensitivity and figure of merit (FoM) of this device as a sensor can reach 950 nm per refractive index unit (nm/RIU) and 161 RIU^{-1}, respectively. Compared with the previous near-infrared sensor, the performance of this sensor has been improved, indicating that it is a simple alternative to the previous high-performance and complex structures.

2. Structure and theory

As shown in Fig. 1(a), the symmetric dual-Tamm structure proposed in this paper contains two identical Ag-DBR structural units. The Ag-DBRs of the two Tamm units is connected to form a symmetric structure. The TE wave (the electric field is parallel to the x axis) incident vertically from the left side of the model structure along the z axis. The whole structure from left to right is Ag-DBR-DBR-Ag structure and a thin layer of ZnO and Ag substrate. The thickness of ZnO is 12 nm. The thickness of the silver substrate must be far greater than the transmission depth of the incident wave to make the transmitted light zero. In the Ag-DBR-DBR-Ag structure, the metal material is Ag, whose thickness is t_m=27 nm. The dielectric constant is expressed by Drude model [16]:

$$\varepsilon_r = \varepsilon_\infty - \frac{\omega_p^2}{\omega^2 + i\omega\gamma} - \frac{\Delta \times \Omega^2}{(\omega^2 - \Omega^2) + i\Gamma}, \tag{1}$$

where ε_∞=2.4064 is the dielectric constant when the incident light frequency ω tends to infinity, ω_p=2π×2214.6×10^{12} Hz, γ=2π×4.8×10^{12} Hz are plasma frequency and collision frequency respectively. Δ=1.6604 is the weight coefficient of the Lorentz term. Ω=2π×620.7×10^{12} Hz is the intensity of Lorentz resonator, Γ = 2π×1330.1×10^{12} Hz is the spectral width of vibration.

The single DBR structure consists of low refractive index silica (SiO_2) and high refractive index titanium dioxide (TiO_2) alternately, and the period number is N. The refractive index of the two materials are n_a=1.45 and n_b=2.6, respectively. The thickness of SiO_2 and TiO_2 layer satisfies Bragg reflection condition: d_a=λ_M /4n_a, d_b=λ_M /4n_b, where λ_M=1700nm is the central wavelength of DBR. Since the TE polarized light is incident from the left side, in order to effectively excite TPP, the material with high refractive index should be selected to connect with the metal. Therefore, the material connected with the Ag layer is TiO_2 layer with d=136 nm. This structure can effectively stimulate the TPP mode.

Figure 1(b) shows the three absorption peaks of TPP mode generated by the structure when N=3, and the TPPs mode will also be coupled with each other. The wavelengths of the three TPP peaks in this band are 1606 nm, 1682 nm, and 1784nm, respectively, whose corresponding absorption rate is 93.907%, 99.822% and 91.128%. Figure 1(c) is the electric field distribution corresponding to the three absorption peaks of TPP mode. It can be seen from Fig. 1(c) that a strong TPP constraint electric field is formed between the Ag film and DBR, which constrains the energy in the structure and improves the absorption capacity of the structure. Figure 1(d) studied the influence of the number of periods N in the DBR structure on the multi-peak absorption spectrum. When N=3, there are three almost completely TPP absorption peaks at 1500~1800nm. With the increase of N, the absorption peaks on both sides move to the center. When N≥5, the left Tamm peak gradually weakens, and until N=7, the left TPP peak basically disappears. When N≥9, the right resonance peak becomes smaller, until N=14, the right resonance peak disappears,

Optical Materials EXPRESS

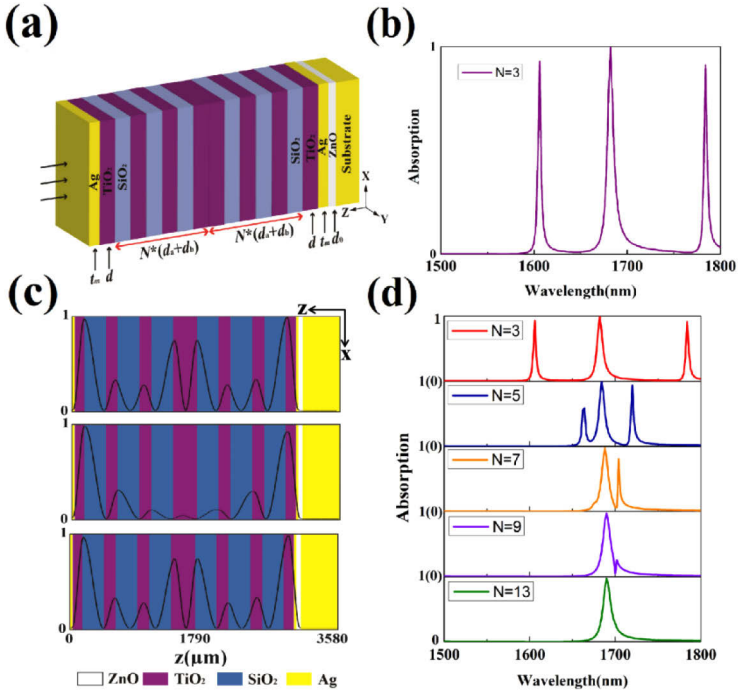

Fig. 1. Design parameters and performance of symmetrical dual-Tamm structure. (a) Dual-Tamm structure. (b) Absorption spectrum of incident light wave in near-infrared band. (c) Electric field distribution in the structure at three absorption peaks wavelength. (d) Effect of different DBR period number N on the absorption spectrum in the structure.

and there is only an intermediate resonance peak in this structure. Therefore, TPP resonance peaks can be adjusted by changing the period number N of DBR in the structure.

The transmission characteristics of the Ag-DBR-DBR-Ag part of the structure can be analyzed by the transmission matrix method (TMM) [17]:

$$E_{\text{out}} = ME_{\text{in}}, \tag{2}$$

where E_{out} is the electric field of the output light, E_{in} is the electric field of the incident light, M is the light transfer matrix in the structure, which is expressed as follows:

$$M = \begin{bmatrix} M_{11} & M_{12} \\ M_{21} & M_{22} \end{bmatrix} = \mathrm{m_{Ag}m_D(m_{SiO_2}m_{TiO_2})^N(m_{TiO_2}m_{SiO_2})^N m_D m_{Ag}} \tag{3}$$

where m_{Ag}, m_{D}, m_{SiO2} and m_{TiO2} are the transmission matrix of light passing through each layer, and N is the period number of DBR.

The transmission matrix of incident light in each layer can be expressed as

$$m_i = \begin{bmatrix} \cos\delta_i & -ip_i^{-1}\sin\delta_i \\ -ip_i\sin\delta_i & \cos\delta_i \end{bmatrix} \tag{4}$$

where $\delta_{\text{i}}=(2\pi/\lambda)n_{\text{i}}d_{\text{i}}\cos\theta_{\text{i}}$, $n_{\text{i}}d_{\text{i}}$ is the optical thickness of the corresponding layer, θ_{i} is the angle between the light in the dielectric layer and the normal direction of the interface, and λ is the wavelength of the incident light.

Optical Materials EXPRESS

When the incident light is incident with TM or TE polarization, the corresponding p_i has the following formulas:

$$p_{i\text{-}TM} = n_i\sqrt{\varepsilon_0\mu_0}/\cos\theta_i \tag{5}$$

$$p_{i\text{-}TE} = n_i\sqrt{\varepsilon_0\mu_0}\cos\theta_i \tag{6}$$

where i = m_{Ag}, m_D, m_{SiO2} or m_{TiO2}, ε_0 and μ_0 are the permeability of vacuum dielectric constant and vacuum dielectric constant respectively.

The reflection coefficient r and the transmission coefficient t of light can be expressed as

$$r = \left|\frac{(M_{11}+M_{12})p_0 - (M_{21}+M_{22}p_t)}{(M_{11}+M_{12})p_0 + (M_{21}+M_{22}p_t)}\right| \tag{7}$$

$$t = \left|\frac{2p_0}{(M_{11}+M_{12}p_t)p_0 + (M_{21}+M_{22}p_t)}\right| \tag{8}$$

where subscript *0* represents the incident space, and subscript *t* represents the transmission space. Therefore, the reflectivity R and transmittance T of the optical absorber can be calculated by the following formula:

$$R = r^2 \tag{9}$$

$$T = \frac{p_t}{p_0}t^2 \tag{10}$$

Therefore, the absorption rate can be calculated by A=1-R-T. Because the bottom of the structure is Ag material, the transmittance T of the structure is basically zero, and the simplified absorption formula is A=1-R.

Figure 2 discusses the influence of structural parameters on the resonant peak. We define the thickness of TiO_2 layer which intersects with Ag layer as d. It can be seen from Fig. 2(a) that with the increase of d, the three resonance peaks have undergone relatively obvious red shifts. By comparison, it can be concluded that the three peaks at d=136 nm have better comprehensive absorption effect and higher absorption. Therefore, the structural parameters are d=136 nm. It can be seen from Fig. 2(b) that with the increase of Ag layer thickness t_m, the three absorption peaks have a very slight red shift, which can be ignored, but the first resonance peak decreases slightly. Therefore, considering the peak of the three resonance peaks, t_m=27 nm is selected as the silver layer thickness of the structure.

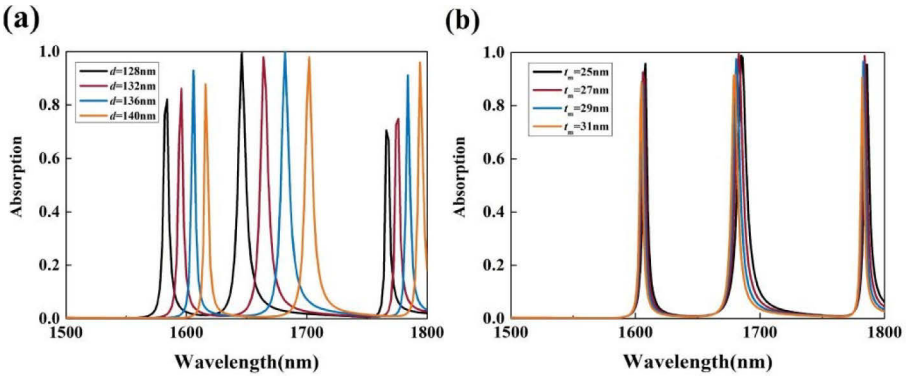

Fig. 2. Influence of structural parameters of materials on both sides of the TPP occurrence interface on these three absorption peaks. (a) Effect of thickness of TiO_2 layer adjacent to DBR on absorption. (b) Effect of Ag thickness on absorption.

Optical Materials EXPRESS

3. Results and discussion

Figure 3(a) shows a hybrid Tamm structure of the absorber with a graphene-based grating added onto the basic structure. The structure has two different resonance modes to achieve multiple absorption peaks. In addition to enhancing the absorption of GMR peaks, the graphene monolayer, sandwiched between the grating and a dielectric layer of SiO_2 can increase the tunability of the structure. Here we set the grating constant (also called the grating period) P=1.15 μm, the thickness and width of the opaque part are h=0.4 μm and W=0.25 μm respectively, and the dielectric matching layer thickness d=1 μm. The excellent photoelectric properties of graphene have been verified in many studies. Usually, the default graphene monolayer is a kind of ultrathin layer, its thickness is T_g=0.34 nm [18], its dielectric constant can be calculated by the following formula [19,20]:

$$\varepsilon_g = 1 + \frac{i\sigma_g}{\omega\varepsilon_0 t_g}, \tag{11}$$

where σ_g is the surface conductivity of graphene, ω is the incident wave, and ε_0 is the vacuum dielectric constant. Since the chemical potential μ_c has a great influence on the dielectric constant, we set the chemical potential of 0.3 eV in this work. Moreover, according to the characteristics of graphene in the near-infrared band as a lossy material, GMR can be used to enhance its absorption [21–23]. At the same time, the GMR mode excited by grating can be coupled with the TPP mode excited in Tamm structure [24].

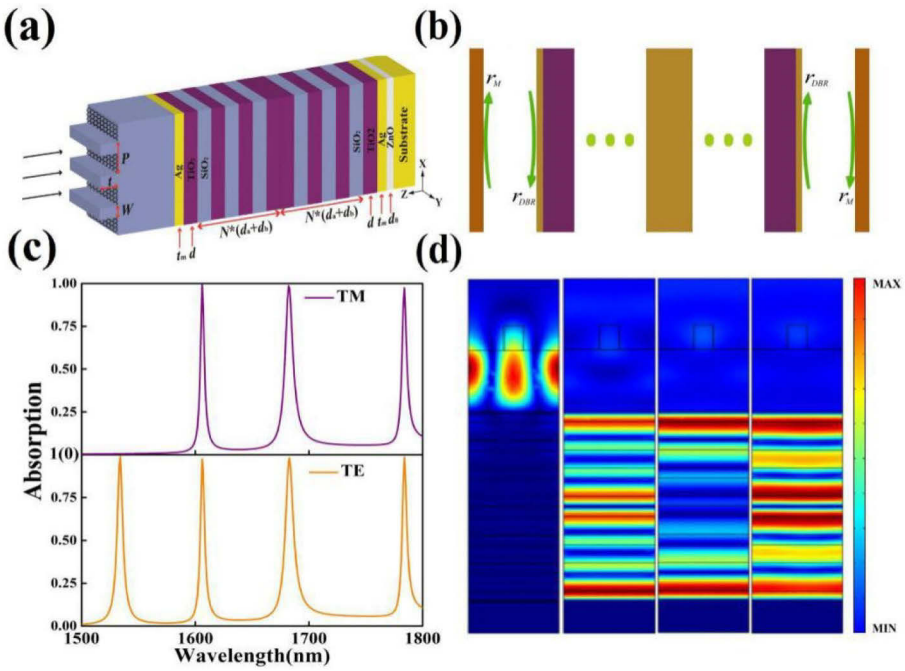

Fig. 3. The design and simulation results of the hybrid Tamm structure with graphene-based grating. (a) The structural parameters of the hybrid structure. (b) The theoretical F-P cavity model is related to TPP mode. (c) The absorption spectrum under the excitation of TM/TE wave. (d) The electric field distribution corresponding to the four absorption peaks excited by the TE wave.

Figure 3(b) exhibits the F-P cavity resonance theoretical model of Tamm plasma resonance [25]. Figure 3(c) shows the absorption spectra generated under normal incident TM and TE polarized light, respectively. The electric vector of the incident light parallel to the incident

Optical Materials EXPRESS

plane is TM polarization, and it is TE polarization if the electric vector of the incident light is perpendicular. Here we consider the x-z section in the COMSOL simulation. So we set the electric field component in the x and z directions to indicate TM polarization, and set the out-of-plane electric field component in the y-direction to indicate TE polarization. The purple line spectrum demonstrates that there are three obvious TPP resonance peaks at 1606 nm, 1682 nm, and 1784nm, corresponding to Tamm states, respectively. The yellow line spectrum illustrates that there is a GMR peak at 1524 nm on the left side of the three TPP peaks, and the absorption efficiency of these four peaks is close to the perfect absorption. After calculation and simplification, the incentive condition should meet the following condition [26]:

$$r_M r_{DBR} \exp(2i\delta) = 1, \tag{12}$$

where r_{M} is the amplitude reflection coefficient of the wave incident by the DBR on the silver layer, and $r_{\mathrm{M}}=(n_{\mathrm{b}}\text{-}n_{\mathrm{a}})/(n_{\mathrm{b}+}n_{\mathrm{a}})$ is given by the Fresnel formula. r_{DBR} is the reflection coefficient of incident wave on DBR, which can be calculated by TMM theory. δ is the phase transition between interfaces. Taking δ=0, the three theoretical resonance wavelengths (1606 nm, 1682 nm and 1784nm) are the same as the numerical results under TE polarization.

This phenomenon can be explained by GMR and Tamm plasmon theory. The GMR wavelength should meet the phase matching:

$$k_{GMR} - k_0 \sin\theta = m\frac{2\pi}{P}, \tag{13}$$

where $k_{\mathrm{GMR}} = k_0 \cdot n_{\mathrm{eff}}$ is the wave vector of the guided mode, and n_{eff} is the effective refractive index of the guided mode. λ is the wavelength, k_0 is the wave number, $k_0=2\pi/\lambda$, m is the diffraction level. In particular, when θ=0, m=1, the above formula can be simplified as $\lambda=n_{\mathrm{eff}}\cdot P$. The electric field distribution wavelength at resonance formation is shown in Fig. 1(c). We can see the resonance mainly occurs in the SiO_2 layer and form a typical standing wave profile. This is to say, GMR will occur if the incident wave is well coupled to the leakage-oriented mode.

To further illustrate the role of TPP in the system model, in Fig. 3(d), we compare the |E| distribution in z-direction at 1606 nm, 1682 nm and 1784nm, respectively. It is found that the three TPPs form a strong TPP-constrained electric field between the silver film and DBR, which greatly reduces the reflection light and enhances the absorption of the system. Among them, TPP I and TPP III also formed a strong TPP-constrained electric field between the two DBR structures, and also played a certain role in strengthening.

After obtaining a four-channel perfect absorption structure, we studied the performance of the structure as a refractive index sensor. We explore the sensitivity and quality factor (FoM) of the sensor structure. The refractive index sensitivity S is an important index to measure the sensor, which is defined as the offset of resonant wavelength corresponding to the change of unit refractive index, and the expression is [27]:

$$S = \frac{\Delta\lambda_{res}}{\Delta n}, \tag{14}$$

where $\Delta\lambda_{\mathrm{res}}$ is the variation of resonant wavelength and Δn is the variation of refractive index. In addition, the FoM is another indicator to evaluate the performance of the sensor. The larger the index is, the better the sensing performance is. The expression is [28]:

$$f_{FoM} = \frac{S}{f_{FWHM}}, \tag{15}$$

where f_{FWHM} is the full width of half peak of resonance peak and S is refractive index sensitivity.

For the structure of this paper, the excitation mode of hybrid graphene-based grating is GMR mode, and the excitation mode of Tamm structure is TPP mode. Therefore, for the GMR peak,

Optical Materials EXPRESS

the SiO2 substrate in the grating part of the structure is selected as the ambient layer, whose refractive index is redefined as nA1. And for the TPP peak, the TiO2 layer connected with the Ag layer is selected as the ambient layer, whose refractive index is redefined as nA2. When the refractive index of the ambient layer changes due to changes in the sample concentration or substance, it can be seen in Fig. 4, GMR peak and TPP peaks have different degrees of red shift. This clearly shows that as the expected performance of the self-reference refractive index sensor, the resonant peak is sensitive to the change of the ambient refractive index.

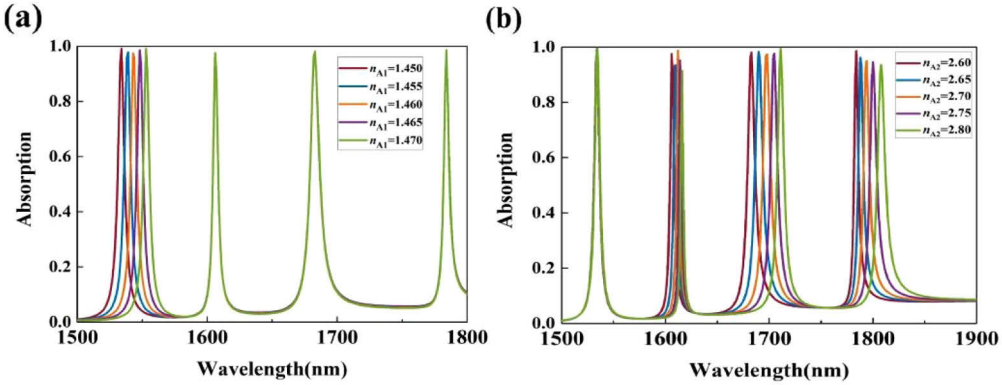

Fig. 4. Effect of refractive index change of the ambient layer on the absorption peak. (a) Effect of refractive index change of corresponding ambient layer on GMR peak. (b) Effect of refractive index change of corresponding ambient layer on TPP peak.

At the same time, the position of the other resonant peak remains unchanged, which can provide the reference frequency. In practical sensor applications, once the structure is designed, the refractive index of the dielectric layer will no longer change. So our proposed sensor structure diagram are shown in Fig. 5. The incident light enters the grating from the left at a certain angle, and the refractive index of the ambient layer changes with the change of the injected gas or liquid sample concentration, thereby affecting the overall absorption spectrum.

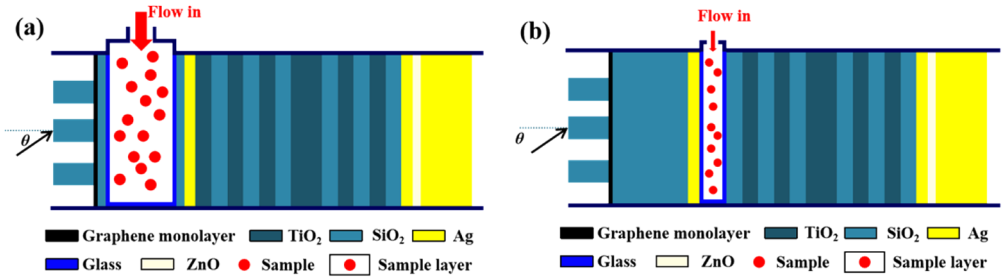

Fig. 5. (a) A schematic diagram of the application after sampling the grating medium layer as the structure of the ambient layer. (b) A schematic diagram of the application after sampling the high refractive index layer near the top Ag layer in the Tamm structure as the ambient layer structure.

After determining that the structure can be used as a refractive index sensor, we studied the influence of its structural parameters on the sensor performance. Since the generation mechanisms of GMR and TPP absorption peaks are different, this paper discusses them separately. For grating, we change the duty ratio by changing the parameter *W*. Figure 6(a) is the influence on GMR. It can be seen that when *W* decreases, the peak of GMR has slightly blue shift, and the offset

Optical Materials EXPRESS

decreases with the increase of W. Figure 6(b) depicts the sensitivity and FoM for different W values. It can be concluded that the grating duty ratio does not affect the sensitivity of GMR peak, and the sensitivity is stable at 950 nm/RIU. In addition, the grating duty cycle, which changed by W, affects FoM.

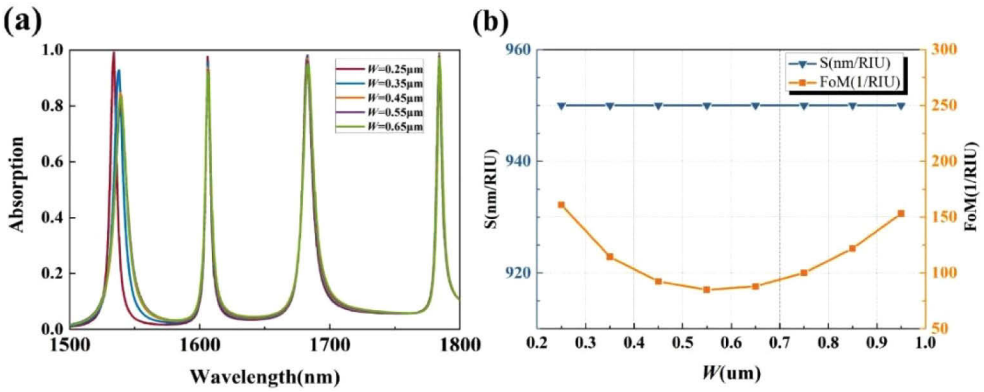

Fig. 6. (a) Effect of graphene grating parameters W on the single-channel excited by GMR in the sensor. (b) Effect of graphene grating parameters W on the sensitivity and quality factor of the GMR peak of the sensor.

We studied the effects of central wavelength parameters λ_M and ambient layer thickness d_1 on TPPs peak in Tamm structure. As shown in Fig. 7(a), when the central wavelength λ_M increases, the three TPP absorption peaks all move blue and the peaks are almost unchanged, but the degree of movement is slightly different, so the sensing performance of the three peaks can be compared. In Fig. 7(b), with the increase of ambient layer thickness d_1, the three TPP absorption peaks also have a blue shift, especially peak 2 and peak 3 moved to a larger extent.

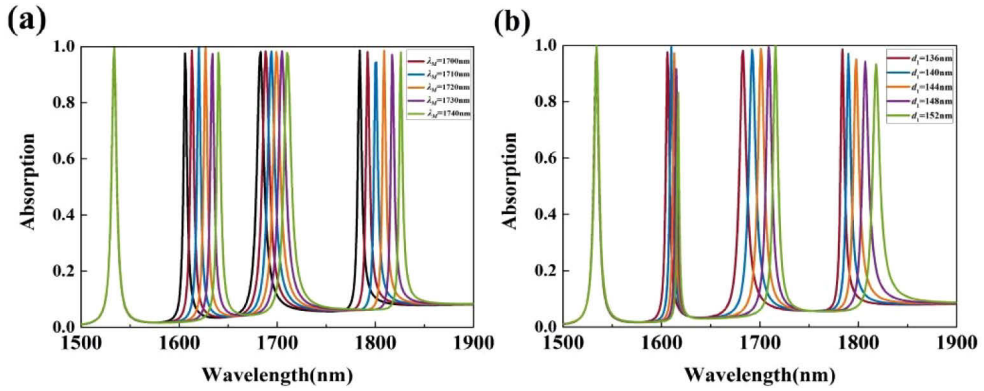

Fig. 7. Fig. Influence of structural parameters of DBR on sensor performance. (a) Influence of central wavelength λ_M, which totally decide DBR structure parameters, on three channels excited by TPP mode in sensor. (b) Influence of thickness of ambient test layer d_1 on three TPP peaks in sensor

The sensor sensitivity and FoM for different λ_M and d_1 are plotted in Fig. 8. And Fig. 8(a) shows the sensitivities of the three TPP peaks at different λ_M. It can be seen that sensitivity of peak 2 is slightly optimized with the increase of λ_M, but the sensitivity of peak 3 is decreasing. Meanwhile, that of peak 1 will not change due to λ_M. FoM corresponding to these three peaks are shown in Fig. 7(b), which displays the FoM fluctuation of peak 2 increases while that of peak

Optical Materials EXPRESS

3 decreases owing to an increase of λ_M. Peak 1 has a downward trend and then tends to be stable, but the overall changes of the three peaks are small. Therefore, λ_M has a little effect on sensor performance. Figure 8(c) illustrates the sensitivity of three TPP peaks at different d_1 values. It can be seen that with the increase of d_1, the sensitivity of peak 3 increases significantly, but the sensitivities of peak 1 and peak 2 decreases. Figure 8(d) is the quality factor corresponding to the three peaks in Fig. 8(c). With the increase of d_1, the FoM of peak 3 increases slightly, while that of peak 1 decreased greatly, and peak 2 changed slightly in a small range. Therefore, the d_1 parameter can significantly optimize the sensing performance of peak 3, and the maximum sensitivity can reach 280 nm/RIU.

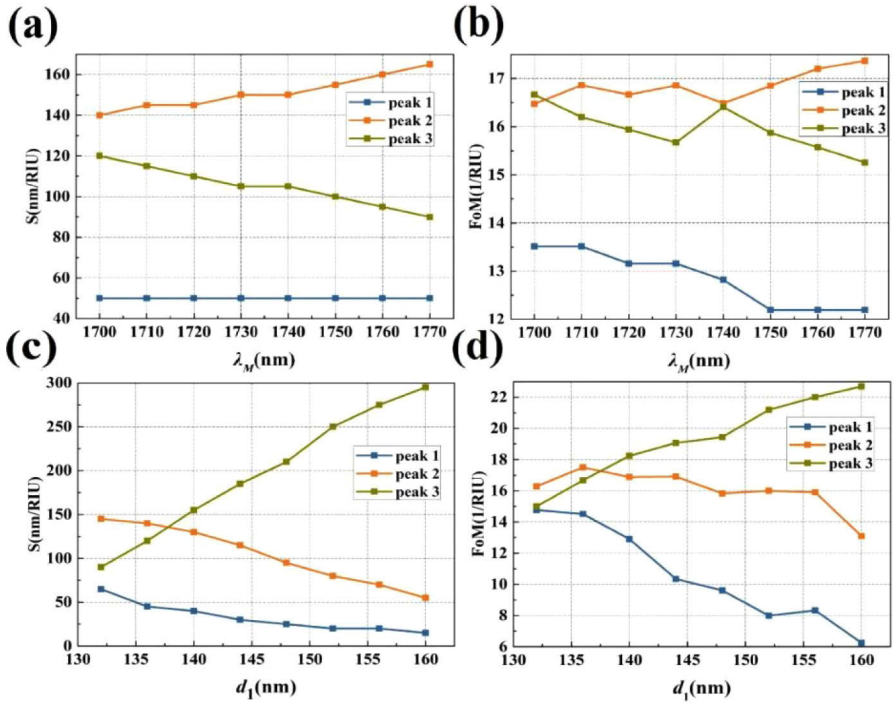

Fig. 8. Effects of DBR parameters on sensor sensitivity and FoM. (a) Effects of central wavelength λ_M on sensor TPP peak sensitivity. (b) Effects of central wavelength λ_M on FoM of sensor using TPP peaks.(c) Effects of ambient layer thickness d_1 on sensitivity of sensor using TPP peaks. (d) Effects of ambient layer thickness d_1 on FoM of sensor.

In Table 1, the performance of the proposed refractive index-sensor is compared with that of the previously proposed near-infrared refractive-index sensor. By comparing the refractive-index sensors with different excitation mechanisms and structures, it can be seen that the proposed sensor has high sensitivity and good FoM. At the same time, it does not need to meet the phase matching condition in the refractive index sensing, which requires lower sensing conditions, and also provides four-channel absorption sensing. It can be seen that the proposed structure has high practical value and can be applied to refractive index detection.

Optical Materials EXPRESS

Table 1. Comparison of previous refractive index sensors with our proposed structures.

Refence	Mechanism	Structure	Max Sensitivity (nm/RIU)	Max FoM (RIU^{-1})
[29]	LSPR	optical fiber	517 (Experiment)	None
[30]	BICs	PhC metasurface	178 (Experiment)	445 (Experiment)
[31]	TPPs	TPP Structure	416 (Simulation)	682 (Simulation)
[32]	SPR	double-layer graphene nanograting (GNG)	430.91 (Simulation)	174.68 (Simulation)
[33]	/	Hybrid dielectric-metal metasurface	840 (Simulation)	84 (Simulation)
[34]	LSPP + PSPP	metal-dielectric-metal shell-core nanorod array + metal film	784 (Simulation)	None
[35]	LSPRs	two-dimensional (2D) gold nanoparticle arra	250 (Simulation)	28 (Simulation)
[36]	LSPRs	periodic gold nanorings array	577 (Experiment)	6.1 (Experiment)
This work	TPPs + GMR	graphene-based grating + dual-Tamm structure	950 (Simulation)	161 (Simulation)

4. Conclusion

We propose a graphene-based hybrid Tamm plasmonic structure for refractive-index sensor. This structure can achieve multi-channel perfect absorption in the near-infrared, based on GMR and TPP. By simulating and optimizing the period number of the DBR in the structure, the grating structure parameters, etc., better sensor performance can be obtained. When the refractive index of the ambient layer in the structure changes, the position of the corresponding absorption peak changes. The optimized sensor has a sensitivity of 950 nm/RIU and FOM of 161/RIU, so it has good sensor performance. Comparing with other high-performance sensors of different types, it was shown that the proposed sensor has a competitive sensitivity and FoM, while it is a simple structure that does not need polarization matching devices, such as prisms or gratings.

Funding. Undergraduate Research and Innovation Projects of China (2020366Y); Open Fund of State Key Laboratory of Applied Optics (SKLAO2020001A04); Intergovernmental Science and Technology Regular Meeting Exchange Project of Ministry of Science and Technology of China (CB02-20); National Natural Science Foundation of China (11811530052).

Disclosures. The authors declare that there are no conflicts of interest related to this article.

Data availability. The data that support the findings of this study are available from the corresponding author upon reasonable request.

References

1. X. Wang, X. Jiang, Q. You, J. Guo, X. Dai, and Y. Xiang, "Tunable and multichannel terahertz perfect absorber due to Tamm surface plasmons with graphene," Photonics Res. **5**(6), 536 (2017).
2. I. Tamm, "Über eine mögliche Art der Elektronenbindung an Kristalloberflächen," Z. Physik **76**(11-12), 849–850 (1932).
3. H. Ohno, E. E. Mendez, J. A. Brum, J. M. Hong, F. Agulló-Rueda, L. L. Chang, and L. Esaki, "Observation of Tamm states in superlattices," Phys. Rev. Lett. **64**(21), 2555–2558 (1990).
4. A. V. Kavokin, I. A. Shelykh, and G. Malpuech, "Lossless interface modes at the boundary between two periodic dielectric structures," Phys. Rev. B **72**(23), 233102 (2005).
5. K. Zhang, Y. Liu, F. Xia, S. Li, and W. Kong, "Tuning of the polariton modes induced by longitudinal strong coupling in the graphene hybridized DBR cavity," Opt. Lett. **45**(13), 3669 (2020).
6. K. L. Zhang, F. Wang, Y. J. Rao, and Y. Jiang, "Novel sensing concept based on optical Tamm plasmon," Opt. Express **22**(12), 14524–14529 (2014).

Optical Materials EXPRESS

7. B. Auguié, M. C. Fuertes, P. C. Angelomé, N. L. Abdala, G. J. A. A. Soler-Illia, and A. Fainstein, "Tamm plasmon resonance in mesoporous multilayers: toward a sensing application," ACS Photonics **1**(9), 775–780 (2014).
8. S. Kumar, M. K. Shukla, P. S. Maji, and R. Das, "Self-referenced refractive index sensing with hybrid-Tamm-plasmon-polariton modes in sub-wavelength analyte layers," J. Phys. D: Appl. Phys. **50**(37), 375106 (2017).
9. J. Hu, M. Li, Z. Wang, Z. D. Hu, J. Wang, S. G. Khakhomov, and I. Semchenko, "High-performance terahertz refractive index sensor based on hybrid graphene Tamm structure," J. Opt. Soc. Am. B **38**(9), 2543–2550 (2021).
10. P. S. Maji, M. K. Shukla, and R. Das, "Blood component detection based on miniaturized self-referenced hybrid Tamm-plasmonpolariton sensor," Sensors and Actuators B: Chemical **255**, 729–734 (2018).
11. N. Li, T. Tang, J. Li, L. Luo, P. Sun, and J. Yao, "Highly sensitive sensors of fluid detection based on magneto-optical optical Tamm state," Sensors and Actuators B: Chemical **265**, 644–651 (2018).
12. X. Zhang, X.-S. Zhu, and Y.-W. Shi, "An optical fiber refractive index sensor based on the hybrid mode of Tamm and surface plasmon polaritons," Sensors **18**(7), 2129 (2018).
13. A. M. Ahmed and A. Mehaney, "Ultra-high sensitive 1D porous silicon photonic crystal sensor based on the coupling of Tamm/Fano resonances in the mid-infrared region," Sci Rep **9**(1), 6973 (2019).
14. B. Roy, S. Majumder, and R. Chakraborty, "Design of low loss surface plasmon polariton waveguide and its use as hybrid Tamm sensor with improved sensitivity," Opt. Eng. **59**(01), 1–11 (2020).
15. Y. Long, L. Shen, H. Xu, H. Deng, and Y. Li, "Achieving ultranarrow graphene perfect absorbers by exciting guided-mode resonance of one-dimensional photonic crystals," Sci. Rep. **6**(1), 32312 (2016).
16. H. Lu, X. Gan, B. Jia, D. Ma, and J. Zhao, "Tunable high-efficiency light absorption of monolayer graphene via Tamm plasmon polaritons," Opt. Lett. **41**(20), 4743–4746 (2016).
17. J. Chilwell and I. Hodgkinson, "Thin-films field-transfer matrix theory of planar multilayer waveguides and reflection from prism-loaded waveguides," J. Opt. Soc. Am. A **1**(7), 742–753 (1984).
18. F. Bonaccorso, Z. Sun, T. Hansan, and A. C. Ferrari, "Graphene photonics and optoelectronics," Nat. Photonics **4**(9), 611–622 (2010).
19. A. Vakil and N. Engheta, "Transformation optics using graphene," Science **332**(6035), 1291–1294 (2011).
20. J. Wang, C. Song, J. Hang, Z. D. Hu, and F. Zhang, "Tunable Fano resonance based on grating-coupled and graphene-based Otto configuration," Opt. Express **25**(20), 23880–23892 (2017).
21. S. Wang and R. Magnusson, "Theory and applications of guided-mode resonance filters," Appl. Opt. **32**(14), 2606–2613 (1993).
22. J. Wang, L. Yang, Z. D. Hu, W. He, and G. Zheng, "Analysis of graphene-based multilayer comb-like absorption enhancement system based on multiple waveguide theory," IEEE Photonics Technol. Lett. **31**(7), 561–564 (2019).
23. J. Wang, L. Yang, M. Wang, Z. D. Hu, Q. Deng, Y. Nie, F. Zhang, and T. Sang, "Perfect absorption and strong magnetic polaritons coupling of graphene-based silicon carbide grating cavity structures," J. Phys. D: Appl. Phys. **52**(1), 015101 (2019).
24. Y. M. Qing, H. Feng, and T. J. Cui, "Flexible control of light trapping and localization in a hybrid Tamm plasmonic system," Opt. Lett. **44**(13), 3302–3305 (2019).
25. M. Kaliteevski, I. Iorsh, S. Brand, R. A. Abram, J. M. Chamberlain, A. V. Kavokin, and I. A. Shelykh, "Tamm plasmon -polaritons: possible electromagnetic states at the interface of a metal and a dielectric Bragg mirror," Phys. Rev. B **76**(16), 165415 (2007).
26. X. Liu, T. Galfsky, Z. Sun, F. N. Xia, E. C. Lin, Y. H. Lee, S. Kéna-Cohen, and V. M. Menon, "Strong light-matter coupling in two-dimensional atomic crystals," Nat. Photonics **9**(1), 30–34 (2015).
27. W. Wei, J. P. Nong, G. W. Zhang, and Y. Zhu, "An infrared biosensor based on graphene plasmonic for integrated nanofluidic analysis," *Proceedings of SPIE-The International Society for Optical Engineering*, 9278 (2014).
28. J. J. Hu, X. C. Sun, A. Agarwal, and L. C. Kimerling, "Design guidelines for optical resonator biochemical sensors," J. Opt. Soc. Am. B **26**(5), 1036 (2009).
29. H. Ai, N. Michiko, and W. Kazuhiro, "Localized surface plasmon sensor based on gold island films using a hetero-core structured optical fiber," Appl. Opt. **56**(23), 6673–6679 (2017).
30. R. Silvia, Z. Gianluigi, T. Stefania, C. Giuseppe, P. Erika, C. Giuseppe, C. Stefano, R. Ivo, and M. Vito, "Label-free sensing of ultralow-weight molecules with all-dielectric metasurfaces supporting bound states in the continuum," Photonics Res. **6**(7), 726–733 (2018).
31. B. Du, Y. W. Li, D. X. Yang, and H. Lu, "High-performance optical sensing based on electromagnetically induced transparency-like effect in Tamm plasmon multilayer structures," Appl. Opt. **58**(17), 4569–4574 (2019).
32. M. Maleki, M. Mehran, and A. Mokhtari, "Design of a near-infrared plasmonic gas sensor based on graphene nanogratings," J. Opt. Soc. Am. B **37**(11), 3478–3486 (2020).
33. X. Liu, T. Zhang, R. Wan, Y. Xu, C. Zhao, and S. Guo, "Numerical investigation of narrowband infrared absorber and sensor based on dielectric-metal metasurface," Opt. Express **26**(8), 10179–10187 (2018).
34. L. Shi, Q. Tang, Z. Liu, Y. Liu, Y. L. Li, G. Liu, and L. Li, "Tunable dual-band plasmonic perfect absorber and its sensing applications," Opt. Express **36**(10), 2750–2756 (2019).
35. J. Chen, J. Yuan, Q. Zhang, H. Ge, C. Tang, Y. Liu, and B. Guo, "Dielectric waveguide-enhanced localized surface plasmon resonance refractive index sensing," Opt. Mater. **8**(2), 342–347 (2018).
36. S. Wang, X. H. Sun, M. J. Ding, G. D. Peng, Y. L. Qi, Y. L. Wang, and J. Ren, "The investigation of an LSPR refractive index sensor based on periodic gold nanorings array," Appl. Phys. **51**, 045101 (2018).

202.198.37.133 {ts '2022-05-24 07:22:54'}